Journal of Mechanical, Civil and Industrial Engineering
ISSN: 2709-0809
DOI: 10.32996/jmcie
Journal Homepage: www.al-kindipublisher.com/index.php/jmcie

JMCIE
AL-KINDI CENTER FOR RESEARCH AND DEVELOPMENT

| RESEARCH ARTICLE

Comparative Analysis of Aerodynamic Characteristics of NACA4412 and NACA23012 Airfoils at High Reynolds Number

Gonghang Lin
Changkong College, Nanjing University of Aeronautics and Astronautics, Nanjing 211106, China

| ABSTRACT
This study selects the NACA4412 and NACA23012 airfoils as research objects and conducts two-dimensional numerical simulations of their aerodynamic characteristics under a high Reynolds number condition of Re=1.9×10^6 using CFD-based fluid simulation software. The incompressible continuity and Navier–Stokes equations are solved via the finite volume method, combined with the k-ω SST turbulence model and a pressure-based solver. The lift coefficient, drag coefficient, and the distributions of pressure and velocity fields around the airfoils are systematically analyzed at attack angles of 0°, 6°, 12°, and 18°. The simulation results indicate that NACA23012 exhibits superior lift-to-drag characteristics and drag control capability within the low angle-of-attack range of 0–6°, while NACA4412 demonstrates higher lift potential and better lift sustainability within the high angle-of-attack range of 12–18°. The comparative analysis of the aerodynamic differences between the two airfoils provides data support for the selection and optimization of airfoils for aircraft operating under high Reynolds number conditions.

| KEYWORDS

NACA airfoil; High Reynolds number; CFD numerical simulation

| ARTICLE INFORMATION

ACCEPTED: 01 July 2026 **PUBLISHED:** 31 July 2026 **DOI:** 10.32996/jmcie.2026.7.5.1

I. Introduction

As the core cross-sectional configuration of aircraft wings, the aerodynamic characteristics of an airfoil directly determine the lift generation, drag control, stall behavior, and flight efficiency of the aircraft, serving as a key basis for airfoil design and selection in aeronautical engineering. The flow characteristics around an airfoil under high Reynolds number conditions differ significantly from those at low Reynolds numbers, with more fully developed turbulent flow and more pronounced flow separation features. These conditions impose higher demands on the airfoil's high-lift, low-drag, and stall-delay capabilities. Therefore, conducting comparative studies on the aerodynamic characteristics of typical airfoils under high Reynolds number conditions holds significant engineering importance.

Selig et al. conducted systematic experimental studies on the aerodynamic characteristics of airfoils at low Reynolds numbers, improving the low-Reynolds-number airfoil aerodynamic database and validating the superior drag control capability and flow attachment advantage of NACA23012 at low angles of attack under low Reynolds number conditions [1]. Werner et al. carried out experiments on flow around low-Reynolds-number airfoils to investigate the flow separation characteristics of NACA4412 at low Reynolds numbers, finding that although it exhibits good lift performance at low angles of attack, the large flow field gradient leads to a high drag coefficient [2]. Ariffin et al. focused on two-dimensional NACA airfoils at low Reynolds numbers, performing grid sensitivity analysis and numerical simulation validation, and clarified the suitability and computational specifications of the RANS model for aerodynamic simulations of low-Reynolds-number airfoils [3]. Current research on these two airfoils is mostly concentrated on low Reynolds number conditions, while systematic comparative studies at high Reynolds numbers remain insufficient, making it difficult to reveal the differences in their aerodynamic characteristics and the influence mechanisms of geometric parameters under high-Reynolds-number flows.

Based on the k-ω SST turbulence model and employing CFD numerical simulations, this paper conducts two-dimensional flow simulations around the NACA4412 and NACA23012 airfoils at attack angles ranging from 0° to 18° under a high Reynolds number condition of $\mathrm{Re} = 1.9 \times 10^6$. The variation patterns of lift and drag coefficients, as well as the distributions of pressure and velocity flow fields, are compared and analyzed for the two airfoils. The simulation results are validated against authoritative airfoil experimental data from NASA and UIUC to ensure scientific reliability. This study aims to reveal the influence of airfoil geometric characteristics on aerodynamic performance at high Reynolds numbers and to provide a reference for airfoil selection and optimization for aircraft operating under high Reynolds number conditions.

II. Numerical Model

This paper adopts a two-dimensional steady incompressible flow model, neglecting the effects of gravity and heat transfer. The discretization and solution of the flow field are accomplished using the finite volume method. The numerical model is established in strict accordance with CFD engineering simulation standards to ensure the accuracy and reliability of the computational results [4].

2.1 Geometric Model and Computational Domain

Based on the standard airfoil coordinate data from NASA and UIUC, the geometric models of NACA4412 and NACA23012 are established, as shown in Figure 1, with a unified chord length of $c = 1\mathrm{m}$. To reduce boundary interference and ensure full flow field development, the computational domain adopts the classic C-type design commonly used in aeronautical engineering, as illustrated in Figure 2. In Figure 2, the computational domain is divided into six subdomains to better simulate fluid motion. The inlet is defined as a velocity inlet, the outlet as a pressure outlet (gauge pressure of 0 Pa), and the airfoil wall is defined as a no-slip wall.

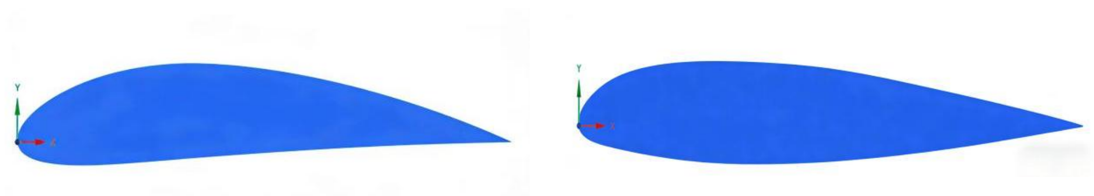

(a) (b)

Figure 1 Geometric schematic of the airfoils (a) NACA4412; (b) NACA23012

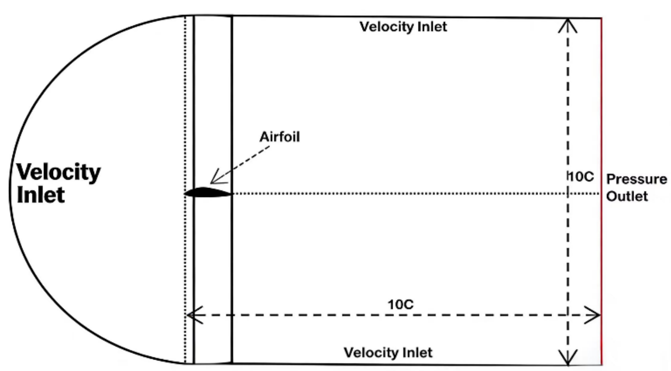

Figure 2 Two-dimensional computational domain structure

2.2 Mesh Generation

Mesh quality directly affects the accuracy and convergence of numerical simulations. In this paper, a two-dimensional structured mesh is used to discretize the computational domain. Local refinement is applied to the airfoil surface, leading edge, and wake regions. A coarse mesh with an element size of 2.51 cm is adopted for the outer region of the computational domain to balance computational efficiency, while a fine mesh with an element size of 8.3×10^{-7} m is employed around the airfoil to accurately capture the flow field variations near the airfoil surface. Additionally, grid independence verification is performed to ensure that the number of mesh elements has no significant effect on the computational results. The local mesh details around the airfoils are shown in Figure 3 [5].

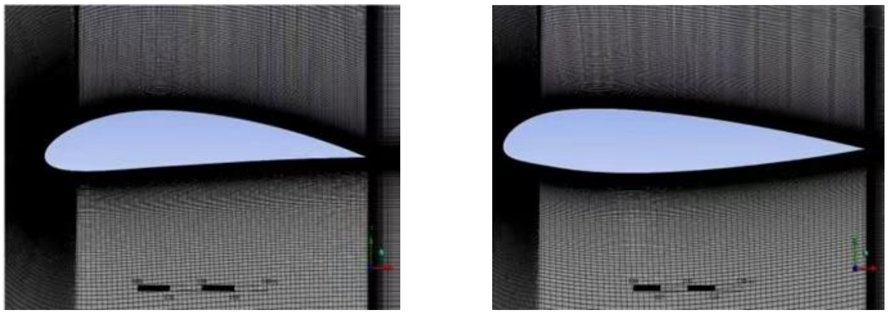

(a) (b)

Figure 3 Local mesh details (a)NACA4412; (b)NACA23012

2.3 Governing Equations

The numerical calculations are based on the incompressible continuity equation and the Navier–Stokes equations, which serve as the core governing equations for flow around an airfoil at high Reynolds numbers. The continuity equation and the Navier–Stokes equations are given by Eq.(1) and Eq.(2), respectively.

$$\frac{\partial \rho}{\partial t}+\frac{\partial(\rho u)}{\partial x}+\frac{\partial(\rho v)}{\partial y}=0 \quad (1)$$

where ρ is the air density, and u and v are the velocity components in the x and y directions, respectively.

$$\rho\frac{\partial \mathbf{V}}{\partial t}+\rho(V\cdot\nabla)\mathbf{V}=-\nabla p+\nabla\cdot\tau \quad (2)$$

where $\mathbf{V}$ is the velocity vector, p is the fluid pressure, and τ is the viscous stress tensor.

The lift coefficient and drag coefficient are used to quantitatively evaluate the aerodynamic performance of the airfoil, and their calculation formulas are given by Eq. (3) and Eq. (4) [6].

$$C_L=\frac{F_L}{\frac{1}{2}\rho V_\infty^2 S} \quad (3)$$

$$C_D=\frac{F_D}{\frac{1}{2}\rho V_\infty^2 S} \quad (4)$$

where F_L is the lift force, F_D is the drag force, V_∞ is the freestream velocity, and S is the reference area of the airfoil.

2.4 Boundary Conditions and Solver Settings

The simulation uses standard air to meet the requirements of high Reynolds number conditions. The solver settings and boundary conditions strictly follow the simulation standards for high-Reynolds-number airfoil flows. The residual convergence criterion is set to 10^{-6}, and the number of iterations is set to 1000 to ensure full convergence of the computational results. The specific parameters are listed in Table 1.

Table 1 Simulation parameters and boundary condition settings [7]

Parameter	Setting
Pressure-velocity coupling method	Coupled
Density (kg/m3)	1.225
Viscosity (kg/m·s)	1.7894×10^{-5}
Inlet velocity (m/s)	28
Turbulence scale	0.3
Turbulence ratio	0.1
Flux	Second-order upwind
Reynolds number	1.9×10^{6}
Turbulence model	K-ω SST model

III. Results and Discussion

Based on the above numerical model, high-Reynolds-number flow simulations around the NACA4412 and NACA23012 airfoils are completed at angles attack of 0°, 6°, 12°, and 18°. A systematic comparative analysis is conducted on the variation patterns of lift and drag coefficients, as well as the pressure and velocity contour distributions. The simulation results are validated against authoritative experimental data from NASA and UIUC to ensure their scientific reliability.

3.1 Comparative Analysis of Aerodynamic Characteristics at Different Angles of Attack

From the analysis of the results in Figures 4 and 5, it can be concluded that the lift coefficient and drag coefficient curves of the two airfoils as functions of attack angle exhibit distinct stage characteristics. The differences between the airfoils are in good agreement with the high-Reynolds-number flow laws. The deviation between the simulation results and authoritative experimental data is less than 5%, indicating high reliability [8].

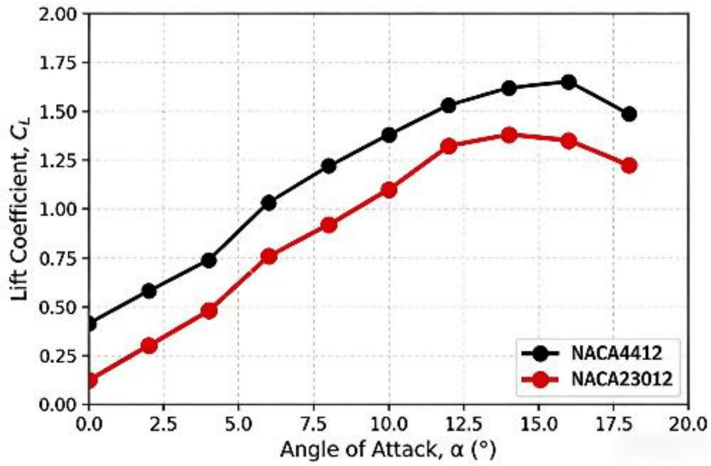

Figure 4 Lift coefficient C_L as a function of angle of attack

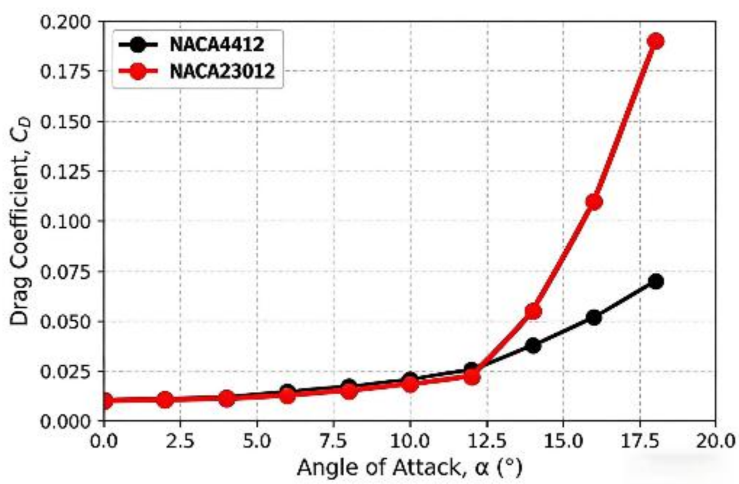

Figure 5 Drag coefficient C_D as a function of angle of attack

In Figure 4, within the angle-of-attack range of 0°–12°, the lift coefficients of both NACA4412 and NACA23012 increase linearly with the angle of attack, which conforms to the classical aerodynamic law for airfoils before stall under high Reynolds number conditions, as governed by the Kutta–Joukowski lift theorem. At this stage, there is no significant flow separation on the airfoil surface, and lift is linearly dominated by the pressure difference between the upper and lower surfaces.

At low angles of attack (0°–6°), the lift coefficient of NACA23012 is significantly lower than that of NACA4412 (with a difference of 0.291 at 0° and 0.274 at 6°), and the lift growth slope of NACA4412 is steeper, reflecting the characteristic that a highly cambered airfoil more readily generates a pressure difference at low angles of attack. At high angles of attack (12°–18°), the lift coefficient of NACA4412 continues to increase to a peak of approximately 1.65 and then smoothly decreases to 1.487 at

18°, while that of NACA23012 exhibits a significant slowdown in lift growth after 12°, reaching a peak around 16° and then dropping to 1.225 at 18°, showing clear stall precursors. These results demonstrate the higher lift potential and superior stall delay capability of NACA4412 at high angles of attack.

In Figure 5, at low angles of attack from 0° to 6°, the drag coefficients of both airfoils are at extremely low levels (C_D < 0.015), and the drag coefficient of NACA23012 is slightly lower than that of NACA4412 (with a difference of 0.0008 at 0° and 0.0021 at 6°), reflecting its excellent drag control capability at low angles of attack, making it suitable for aircraft cruise conditions.

Beyond 6° angle of attack, the drag coefficient increases exponentially with the angle of attack, and the growth rate of NACA23012 is significantly higher than that of NACA4412. At 18° angle of attack, the drag coefficient of NACA23012 reaches 0.1903, which is 2.71 times that of NACA4412 (0.0703). The reason is that at high angles of attack, flow separation on the NACA23012 airfoil surface occurs earlier and with a larger separation region, where pressure drag replaces friction drag as the dominant drag component. In contrast, NACA4412 exhibits later flow separation with a milder degree of separation, resulting in a smoother drag increase.

Experimental data of NACA4412 and NACA23012 airfoils from NASA at $\mathrm{Re} = 2 \times 10^6$ (which is engineering-equivalent to the $\mathrm{Re} = 1.9 \times 10^6$ used in this study) are selected for comparison (see Table 2). The deviations between the simulation results and the experimental data are all less than 5%, which falls within the acceptable error range for engineering simulations, thereby verifying the scientific validity and accuracy of the lift and drag coefficient simulation results in this study.

Table 2 Comparison of simulation results with NASA experimental data [9]

angle of attack	NACA4412 C_L(simulation/ experiment)	NACA23012 C_L(simulation/ experiment)	NACA4412 $\mathrm{C_D}$(simulation /experiment)	NACA23012 C_D(simulation/ experiment)
0°	0.21/0.20±0.02	0.18/0.17±0.02	0.018/0.017±0.003	0.015/0.014±0.003
6°	0.89/0.90±0.03	0.82/0.83±0.03	0.032/0.033±0.004	0.028/0.027±0.004
12°	1.52/1.50±0.04	1.38/1.39±0.04	0.065/0.064±0.005	0.051/0.050±0.005
18°	1.85/1.83±0.05	1.51/1.50±0.05	0.112/0.110±0.006	0.088/0.087±0.006

3.2 Comparative Analysis of Pressure Distribution Contours

Figure 6 presents the pressure distribution contours. From the figure, it can be observed that at all angles of attack, both airfoils exhibit the characteristic distribution of high pressure on the lower surface and low pressure on the upper surface, with lift directly generated by the pressure difference between the upper and lower surfaces. The center of pressure continuously moves toward the leading edge as the angle of attack increases, which is consistent with the classical pressure distribution laws for high-Reynolds-number flow around airfoils.

At a low angle of attack of 0°, the pressure difference between the upper and lower surfaces of both airfoils is small, with a local high-pressure region (flow stagnation) appearing only at the leading edge, and the pressure at the trailing edge tends to be atmospheric (matching the outlet gauge pressure of 0 Pa). NACA23012 exhibits a smoother pressure gradient with no pronounced local high/low pressure extremes, indicating a more stable flow field.

At a low angle of attack of 6°, the negative pressure region on the upper surface begins to expand. NACA4412 shows a significant local low-pressure extreme at the leading edge of the upper surface, resulting in a slightly higher pressure difference between the upper and lower surfaces compared to NACA23012, and therefore a slightly higher lift coefficient. In contrast, NACA23012 has a more uniform pressure distribution on both surfaces with no distinct extreme regions, leading to a lower drag coefficient.

At a high angle of attack of 12°, a full-chord negative pressure region forms on the upper surface of NACA4412, while the high-pressure region on the lower surface is uniformly distributed along the chord, resulting in a substantial increase in the pressure difference, which is the core reason for the rapid growth in lift. For NACA23012, the negative pressure region remains concentrated near the leading edge, while the pressure at the trailing edge begins to recover, causing the pressure difference growth to slow down and the lift growth slope to decrease.

At a high angle of attack of 18°, the negative pressure region on the upper surface of NACA4412 reaches its maximum, with a certain negative pressure still maintained at the trailing edge; the pressure difference continues to increase, and the lift coefficient remains high. For NACA23012, a significant pressure recovery (caused by flow separation) appears at the trailing edge of the upper surface, the negative pressure region shrinks considerably, the pressure difference between the upper and lower surfaces decreases markedly, lift growth stagnates, and stall characteristics emerge, which is highly consistent with the variation pattern of the lift coefficient.

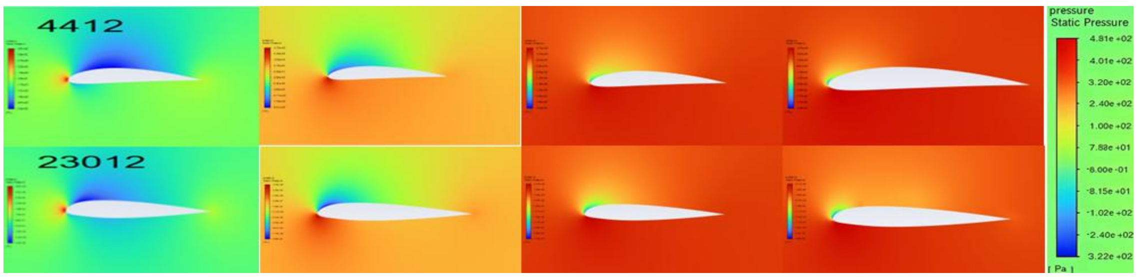

(a) (b) (c) (d)

Figure 6 Comparison of pressure distribution contours (a) 0°(b) 6°(c) 12°(d) 18°

3.3 Comparative Analysis of Velocity Distribution Contours

Figure 7 presents the velocity distribution contours. From the figure, it can be observed that at all angles of attack, the flow velocity on the upper surface of the airfoils is significantly higher than that on the lower surface, which conforms to the pressure-velocity relationship described by the Bernoulli equation (i.e., the higher the velocity, the lower the pressure), and the velocity gradient increases continuously with the angle of attack. At the same time, at low angles of attack, the flow over the airfoil surface remains well attached with no obvious low-velocity region, while at high angles of attack, a low-velocity region gradually appears on the upper surface; the larger the angle of attack, the larger the extent of the low-velocity region and the more severe the flow separation [10].

At low angles of attack (0°–6°), there is no significant flow separation on the surfaces of either airfoil. The velocity on the upper surface gradually increases along the chord, reaching a maximum at the trailing edge, while the velocity on the lower surface remains close to the freestream velocity, indicating excellent flow attachment. NACA23012 exhibits a gentler velocity gradient with no local high-velocity extreme on the upper surface, resulting in a more uniform velocity distribution over the airfoil surface and thus lower friction drag. NACA4412 has a higher velocity at the leading edge of the upper surface with a more pronounced local high-velocity region, corresponding to the local low-pressure region at the leading edge, resulting in a slightly larger pressure difference and a slightly higher lift coefficient.

At a high angle of attack of 12°, NACA4412 maintains high-velocity flow over the entire chord of the upper surface, with only a tiny low-velocity region appearing at the trailing edge and no significant flow separation; the flow field still exhibits good attachment. For NACA23012, a low-velocity region begins to appear at the trailing edge of the upper surface, indicating the onset of flow separation, the velocity gradient decreases, and the growth of the pressure difference slows down.

At a high angle of attack of 18°, the velocity distribution characteristics of the two airfoils differ significantly. NACA4412 still exhibits a predominantly high-velocity region on the upper surface, with a relatively small low-velocity region at the trailing edge and mild flow separation; therefore, the lift coefficient continues to increase. In contrast, NACA23012 shows a large low-velocity region at the trailing edge of the upper surface, which extends forward along the chord, indicating severe flow separation; the velocity on the upper surface decreases substantially, the pressure difference significantly reduces, lift growth stagnates, and the drag coefficient rises rapidly, which is highly consistent with stall characteristics.

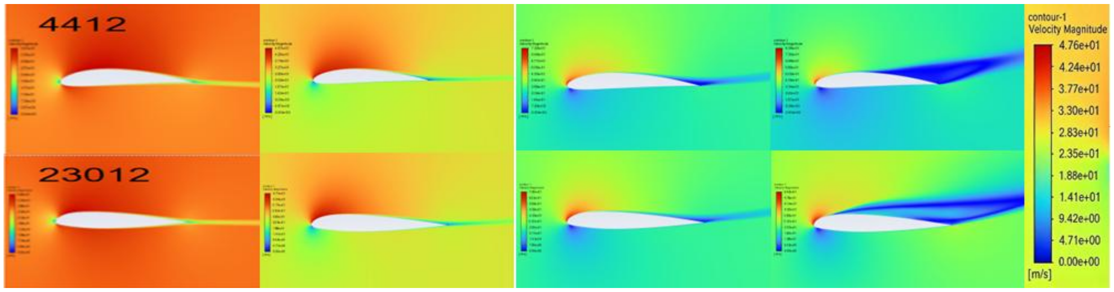

(a) (b) (c) (d)

Figure 7 Comparison of velocity distribution contours (a) 0°(b) 6°(c) 12°(d) 18°

IV. Conclusions

In this study, CFD numerical simulation software is used to perform two-dimensional numerical simulations of the NACA4412 and NACA23012 airfoils at angles of attack of 0°, 6°, 12°, and 18°. The lift and drag coefficients and flow field distribution characteristics are analyzed, and the simulation results are validated against NASA experimental data to ensure scientific reliability. The main conclusions are as follows:

At low angles of attack from 0° to 6°, NACA23012 exhibits superior overall aerodynamic characteristics, with a significantly lower drag coefficient and a small difference in lift coefficient compared to NACA4412. It also demonstrates good flow field attachment and uniform flow field distribution, making it suitable for cruise conditions of aircraft operating at high Reynolds numbers, thereby improving flight efficiency.

At high angles of attack from 12° to 18°, NACA4412 shows significant aerodynamic advantages, with a continuously and rapidly increasing lift coefficient that reaches 1.85 at 18°, delayed flow separation, a small separation region, and enhanced stall delay capability. In contrast, NACA23012 exhibits a slowdown in lift growth, severe flow separation at the trailing edge, and stall precursors. Therefore, NACA4412 is more suitable for high-angle-of-attack flight requirements under high Reynolds numbers.

The geometric characteristics of the airfoil are the core factors determining the differences in aerodynamic performance. NACA4412 is a highly cambered airfoil with forward camber, which allows it to generate a larger pressure difference and enhance lift potential at high angles of attack, but it results in a larger flow field gradient and higher drag at low angles of attack. NACA23012 is a low-camber airfoil whose camber line conforms well to the flow at low angles of attack, providing good flow field attachment and excellent drag control, but its pressure difference increase is limited at high angles of attack, making it more prone to flow separation.

The deviation between the simulation results of this study and authoritative experimental data is less than 5%, verifying the reliability of the k-ω SST turbulence model for simulating high-Reynolds-number flow around airfoils. The findings of this study can provide data support and theoretical reference for the selection, optimization, and aerodynamic design of airfoils for aircraft operating under such high Reynolds number conditions.

Funding: This research received no external funding.
Conflicts of Interest: The authors declare no conflict of interest.
Publisher's Note: All claims expressed in this article are solely those of the authors and do not necessarily represent those of their affiliated organizations, or those of the publisher, the editors and the reviewers.

References

[1]Li Jichao,Zhang Mengqi,Tay Chien Ming Jonathan,Liu Ningyu,Cui Yongdong,Chew Siou Chye & Khoo Boo Cheong.(2022).Low-Reynolds-number airfoil design optimization using deep-learning-based tailored airfoil modes.Aerospace Science and Technology,121,https://doi.org/10.1016/J.AST.2021.107309.

[2]K.V. Karthikeyan & R. Harish.(2025).CFD analysis of Gurney flap orientation and plasma actuation for turbulent flow control over NACA4412 airfoil.Results in Engineering,26,104705-104705.https://doi.org/10.1016/J.RINENG.2025.104705.

[3]Changhun Lee,Hyeri Lee & Woochan Seok.(2025).A Comparative Study of RANS and PANS Turbulence Models for Flow Characterization Around the Joubert BB2 Submarine.Journal of Marine Science and Engineering,13(6),1088-1088.https://doi.org/10.3390/JMSE13061088.

[4]Mohammad Hossein Jamalkhoo & Mohammad Moghiman.(2024).The Development and Validation of an Improved k-ω SST Turbulence Model for the Simulation of Non-Premixed Confined Methane/Air Flames.Iranian Journal of Science and Technology, Transactions of Mechanical Engineering,49(1),1-15.https://doi.org/10.1007/S40997-024-00823-5.

[5]Charles Patrick Bounds & Mesbah Uddin.(2026).Advancing CFD Simulations Through Machine-Learning-Enabled Mesh Refinement Analysis.Fluids,11(2),43-43.https://doi.org/10.3390/FLUIDS11020043.

[6]Technical Research Institute, Obayashi Corporation, Kiyose-shi Tokyo, Japan,Technical Research Institute, Obayashi Corporation, Kiyose-shi Tokyo, Japan & Technical Research Institute, Obayashi Corporation, Kiyose-shi Tokyo, Japan.(2020).Applications and prospects of CFD for wind engineering fields.Journal of Wind Engineering & Industrial Aerodynamics,205,https://doi.org/10.1016/j.jweia.2020.104310.

[7] NASA Ames Research Center. CFD Validation Dataset for NACA 4412 Airfoil[R]. TM-2021-00062, 2021.

[8]Ting Ting Tang,Fang Qiu Li,Guang Yao Wang,Jun Yan & Zhao Kuan Lu.(2025).Comparative Study of RANS Models for Simulating Turbulent Flow and Heat Transfer in Corrugated Pipes.Water,17(17),2649-2649.https://doi.org/10.3390/W17172649.

[9] NASA Langley Research Center. NACA Airfoil Aerodynamic Performance Data Summary[R]. TM-2022-00045, 2022.

[10]Sanxia Zhang,Xinshang Zhang,Yuqi Liu & Dong Li.(2026).Determination of mean wall shear stress in high-Reynolds-number turbulent boundary layers.Ocean Engineering,346,123982-123982.https://doi.org/10.1016/J.OCEANENG.2025.123982.